


Microwave coherent spectroscopy of ultracold thulium atoms

D. A. Pershin,^{1,2} V. V. Yaroshenko,³ V. V. Tsyganok,^{1,4,5} V. A. Khlebnikov,¹ E. T. Davletov,^{1,4} D. V. Shaykin,^{1,4}
E. R. Gadylshin,^{1,4} I. S. Cojocar, ^{1,2,6} E. L. Svechnikov,³ P. V. Kapitanova,³ and A. V. Akimov ^{1,2,6,*}

¹*Russian Quantum Center, Business Center “Ural,” 100A Novaya Street Skolkovo, Moscow 143025, Russia*

²*PN Lebedev Institute RAS, Leninsky Prospekt 53, Moscow 119991, Russia*

³*Faculty of Physics and Engineering, ITMO University, 197101 Saint Petersburg, Russia*

⁴*Moscow Institute of Physics and Technology, Institutskii pereulok 9, Dolgoprudny, Moscow Region 141701, Russia*

⁵*National University of Science and Technology MISIS, Leninsky Prospekt 4, Moscow 119049, Russia,*

⁶*Texas A&M University, TAMU 4242, College Station, Texas 77843, USA*



(Received 27 July 2020; accepted 28 September 2020; published 23 October 2020)

Recently, the thulium atom was cooled down to the Bose-Einstein condensation temperature, thus opening a pathway to quantum simulation with this atom. However, successful simulations require instruments to control and read out states of the atom as well as the ability to control the interaction between either different species or different states of the same type of species. In this paper, we provide an experimental demonstration of high-fidelity (over 93%) manipulation of the ground-state magnetic levels of thulium, which utilizes a simple and efficient design of a microwave (MW) antenna. The coherence time and dephasing rate of the energetically highest hyperfine level of the ground state were also examined.

DOI: [10.1103/PhysRevA.102.043114](https://doi.org/10.1103/PhysRevA.102.043114)

I. INTRODUCTION

Ultracold atoms have become a solid platform for quantum simulations [1–3]. Manipulation of the interatomic interactions in such a simulator can be routinely achieved using so-called Fano-Feshbach resonances [4]. In particular, thulium, having the single bosonic isotope ¹⁶⁹Tm, was recently cooled down to the Bose-Einstein condensation (BEC) temperature [5]. It has relatively large orbital angular momentum and magnetic dipole moment $\mu = 4\mu_B$ in the ground state along with a relatively simple level structure compared to other highly magnetic rare-earth elements [6,7] and could thus be useful $L = 3$ for quantum simulations. In the case of the thulium atom, similar to other rare-earth elements [8–11], Fano-Feshbach resonances are accessible at low (Gauss level) magnetic fields [12].

For quantum simulations, the abilities to manipulate the ground state and to populate specific ground-state components with high fidelity are of great importance. The atoms cooled down to nearly BEC temperature are usually polarized in the ground state [in the presence of a direct current (dc) external magnetic field]; thus, there is a rather pure state with a single level populated [13]. In the case of thulium, the ground state is $|F = 4, m_F = -4\rangle$. A polarization purity in cold atomic gas of well over 95% is experimentally achievable [14]. In the presence of a small external magnetic field, population of other Zeeman levels could be achieved using direct radio-frequency excitation of these transitions [15] via, for instance, resonant π pulses [16]. This method is well established and has been developed into complicated composite pulses

correcting for various errors in π pulses [17–19] as well as the adiabatic rapid passage technique [20]. Nevertheless, the major difficulty with these methods is the necessity of a strong low-frequency field, which often needs to be delivered into a metallic vacuum volume. Additionally, this method is hard to implement in very low or zero magnetic fields. Thus, a Raman-type scheme is often more convenient for such experiments [21,22].

A Raman-type population may, in principle, be realized via optical levels with cautions taken to address two nearly located narrow levels [23], but utilization of the ground-state hyperfine structure microwave (MW) $F = 4 \rightarrow F = 3$ transition with frequency [24,25] seems to be a convenient approach [see Fig. 1(a)] which eliminates possible off-resonant optical excitation and subsequent loss, as well as the requirement for an additional laser field. An additional advantage of this approach is the relatively long lifetime of the intermediate state, enabling cascade excitation instead of the commonly used stimulated adiabatic rapid passage. While this MW radiation still needs to be delivered into a metallic, in our case, vacuum volume, this task is solvable [26].

In this paper, we demonstrate manipulation of the ultracold thulium atom ground state using a Raman-like approach. The manipulation was performed using a specially developed MW antenna. The fidelity of transfer as well as the coherence properties of the intermediate hyperfine structure level was estimated.

II. EXPERIMENTAL SETUP

Thulium atoms were cooled and trapped using a procedure described elsewhere [14,26,27]. The temperature of the cloud was set to $T \simeq 1.6 \pm 0.2 \mu\text{K}$, and the number of atoms in the

*akimov@physics.tamu.edu

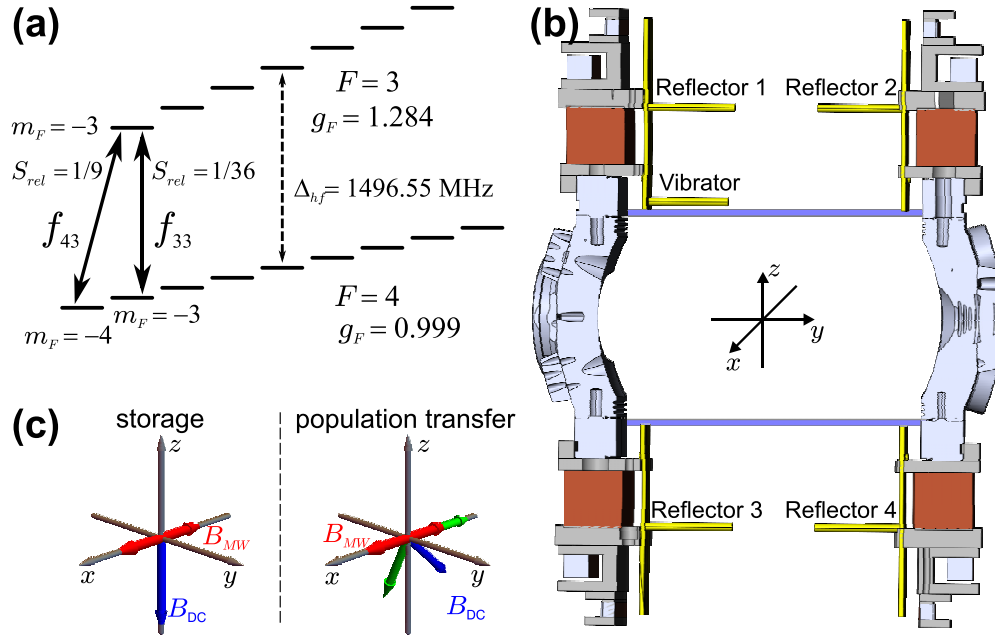


FIG. 1. (a) Level scheme of the thulium atom ground state. F stands for the total atom momentum; m_F for its projection onto the quantization axis (dc magnetic field); S_{rel} for the relative strength of the transition, or square of the 3- j symbol of the transition; f for the transition frequency; g for the Landé g factor; and Δ_{hf} for the hyperfine splitting frequency. (b) Vacuum chamber with MW antenna installed. (c) Orientations of the dc and MW magnetic fields used in the experiments. Green arrows indicate components of the dc magnetic field along the MW magnetic field direction and perpendicular to it.

crossed beam optical dipole trap (532 nm) [5] polarized in the $|F = 4, m_F = -4\rangle$ level was approximately 10^5 . Detection of the atomic cloud was performed via absorption imaging [28], described in detail in the Supplemental Material [29].

The atom polarization was maintained with a vertical dc magnetic field $B = 4.09 \pm 0.04$ G [Fig. 1(c), storage], that is considerably detuned from the closest Feshbach resonance for open channel $|F = 4, m_F = -4\rangle \rightarrow |F = 4, m_F = -4\rangle$ situated at 4.36 G [12] associating the width of the resonance with atomic losses.

In the presence of an external magnetic field, the ground state of $^{169}\text{Tm } 4f^{13} ({}^2F^o) 6s^2 {}^2F_{7/2}^o (I = 1/2)$ (I stands for nuclear spin) splits into Zeeman levels [Figs. 1(a) and 1(c)], which are separated, if one neglects the quadratic Zeeman shift, by frequencies $g_F B \mu_B / \hbar$, where g_F stands for the Landé g factor, B is the magnetic field, \hbar is the Planck constant, and μ_B is the Bohr magneton. The g factors of the hyperfine components of the ground state are $g_{F=4} = 0.999$ and $g_{F=3} = 1.284$ (see Supplemental Material [29]). Since these g factors are different, the magnetic dipole allowed transitions between hyperfine components of the ground state have different frequencies, thus allowing frequency selective addressing of specific transitions with an MW field.

The preparation procedures allow one to polarize atoms in the level $|F = 4, m_F = -4\rangle$ along the external magnetic field [14]. Since the magnetic field creates quantization axes, magnetic dipole allowed transitions could be excited efficiently with circular or linear polarization of the MW field, thus populating any desired state. Experimentally, transitions with frequencies f_{43} and f_{33} were selected because of their reasonably large transition strengths [1/9 and 1/36, respectively; see Fig. 1(a)]. The transitions could thus be excited

with circular and linear polarization, respectively. To address both these polarizations (and potentially a negative circular polarized transition as well), it was decided to use an MW source with a linear MW magnetic field component along the x axis.

To address the transition between hyperfine levels of the ground state, an MW antenna, depicted in Fig. 1(b), was developed. In contrast to the previous version [26], this design has one active (vibrator) and four passive (reflectors) elements. The active vibrator is a conductive element, that converts currents induced in it into microwave radiation. It is a nonsymmetric vibrator that together with the reflector immediately below it can be considered as the simplest Yagi-Uda antenna [30]. The antenna elements are in the yz plane, thus generating an x -polarized magnetic field. The combination of the bottom and top reflectors forms a cavity, which has a resonance frequency close to 1.5 GHz. The antenna has a bandwidth of 10 MHz for the -10 dBm level and a maximum magnetic field in the central region of the vacuum volume (see Fig. 2). We note that, in principle, one could try to use the vacuum chamber itself as a cavity, but unfortunately, its vacuum volume size does not allow excitation of the desired frequency.

Initial optimization of the x component of the MW magnetic field was performed with CST MW Studio Suite 2017. The obtained x component of the magnetic field distribution is presented in Fig. 2. The antenna parameters optimized during the simulations are summarized in Table I. One can see from Fig. 2 that the magnetic field distribution is asymmetric in the xy and yz planes, which can be explained by the asymmetric field excitation. However, the maximum magnetic field is observed in the chamber center, reaching a value of 43 mG.

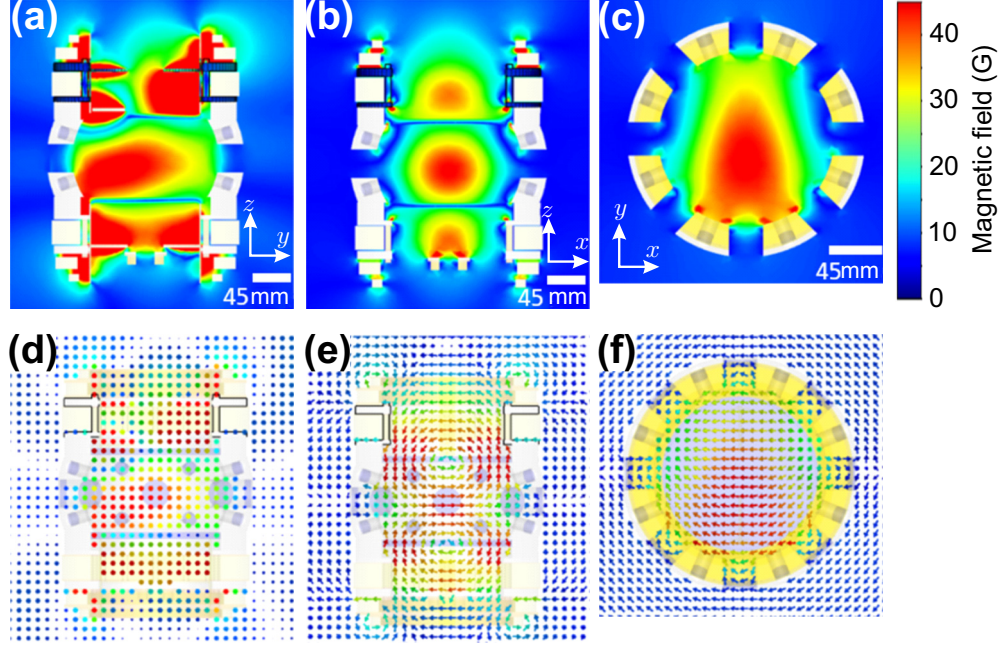


FIG. 2. Numerically calculated distribution of the x component of the MW magnetic field in the vacuum chamber in the (a) yz , (b) xz , and (c) xy planes, and vector distribution of the MW magnetic field in the chamber in the (d) yz , (e) xz , and (f) xy planes.

One may conclude that the antenna efficiently utilizes the excitation power despite the presence of asymmetry. From the vector plot of the magnetic field distribution, one can see that the field has mainly a vertical component (x component). The gradient of the MW magnetic field in the center of the chamber does not exceed 1% per millimeter.

The feeding network of the MW antenna is illustrated in Fig. 3(a). To generate an MW signal, an SG 384 oscillator (Stanford Research Systems, “SRS” in the figure) and the tracking generator of an HMS3010 spectrum analyzer (Rohde and Schwarz, “R&S” in the scheme) were used. The two generators were used to enable fast frequency switching, which was implemented using a ZASWA-2-50DR switch (Mini Circuits). The signal of the sources was modulated with another switch of the same type. The free output of the switch was loaded with 50 Ω . The modulated signal was then amplified with a ZHL-10W-2G+ amplifier (Mini Circuits, “Amp” in the figure) and fed to the antenna. The switches were controlled by a field-programmable gate array [National Instruments NI PCIe-6363, “FPGA” in Fig. 3(a)] and a Stanford Research Systems DG 645 delay generator (“Delay” in the figure),

thus allowing realization of the various pulse schemes demonstrated in Fig. 3(b).

III. RESULTS

To determine the magnitude of the experimentally achieved MW magnetic field, a Rabi oscillation sequence was used [Rabi in Fig. 3(b)], thus allowing observation of the Rabi oscillation at the f_{43} transition frequency [Fig. 3(c)]. The data were fitted with the following dependence of the $|F = 4, m_F = -4\rangle$ level population n_{44} :

$$n_{44} = a[1 + \cos(\Omega\tau)] + b, \quad (1)$$

where a, b are fit parameters, τ is time, and Ω is the Rabi frequency [31]. Since the Rabi frequency depends on detuning Δ as $\Omega = \sqrt{\Omega_{\text{Rabi}}^2 + \Delta^2}$, with Ω_{Rabi} being the resonance Rabi frequency, the detuning was chosen to be 0 by fitting the dependence of the Rabi frequency on the frequency f applied to the transition (Fig. 3(D); see Supplemental Material [29]) with the following function:

$$\Omega = \sqrt{\Omega_{\text{Rabi}}^2 + (f - f_{34})^2}. \quad (2)$$

For this experiment, the direction of the dc magnetic field was kept vertical, as it is set for atom loading and storage in the trap [Fig. 1(c)]. For such an orientation of the field, the atoms experience the maximum possible circular component of the MW field. The MW antenna was tuned within the experimental setup (see Supplemental Material [29]) to reach the maximum allowed by the design Rabi frequency of $\Omega_{\text{Rabi}} = 2\pi \cdot 15.55$ kHz. The magnitude of the ac magnetic field was found to be $B = 21 \pm 1$ mG using the following equation:

$$\vec{B} \cdot \vec{\mu} = \hbar\Omega_{\text{Rabi}}, \quad (3)$$

TABLE I. MW antenna parameters. The source is assumed to be 10 W at 1.5 GHz.

Magnetic field intensity	43 mG
Length of the active vibrator	41.8 mm
Length of reflector 1	48.6 mm
Length of reflector 2	45.5 mm
Length of reflectors 3 and 4	45 mm
Distance between the vibrator and the first reflector	60 mm
Diameter of vibrator/reflectors	4 mm
Material	Brass

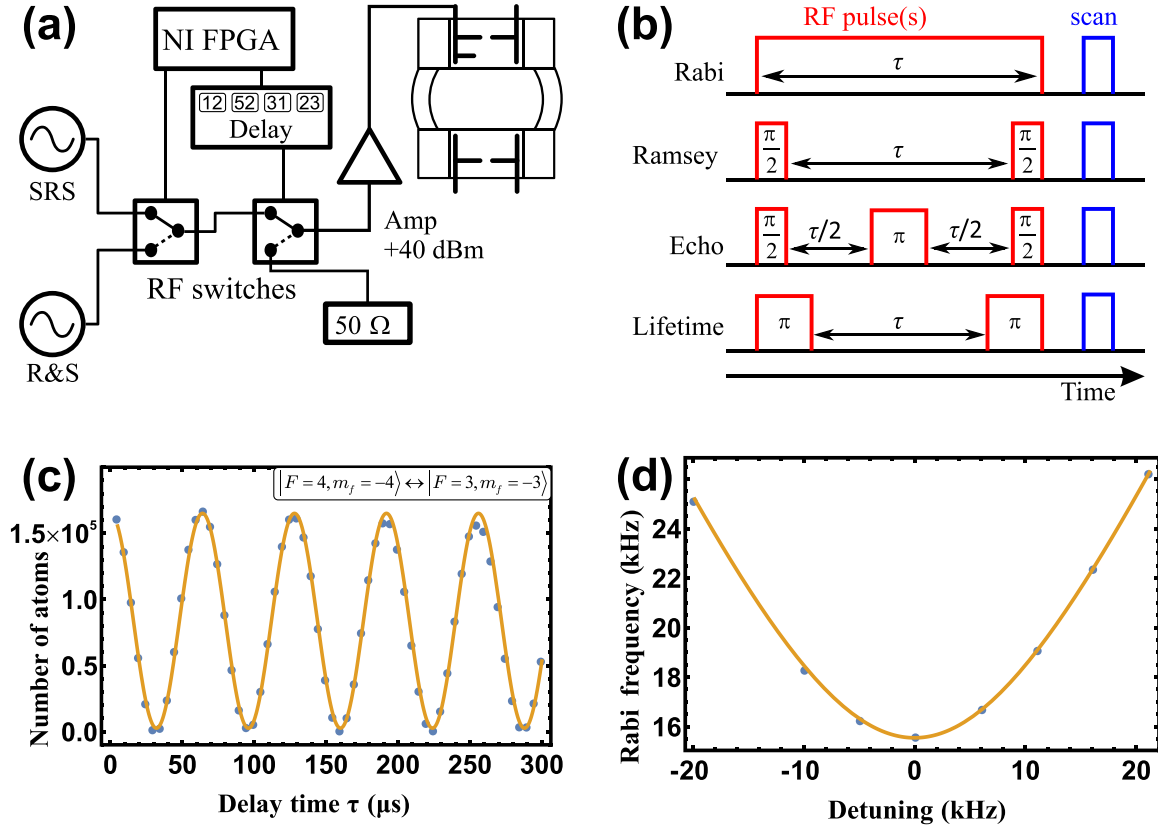


FIG. 3. (a) Diagram of the MW part of the experimental setup. “SRS” stands for Stanford Research Systems SG 384, “R&S” stands for Rohde and Schwarz HMS3010 (generator output), “RF switches” stands for Mini Circuits ZASWA-2-50DR, “Delay” stands for Stanford Research Systems DG645, “Amp” stands for Mini Circuits ZHL-10W-2G+ amplifier, and “NI FPGA” stands for National Instruments NI PCIe-6363. (b) Pulse sequences used for the experiment described in the paper. (c) The data (dots) show the Rabi oscillations of the atomic ensemble for the transition with frequency f_{43} , and the solid line represents the fit function (1) with parameters $\Omega = 2\pi \cdot 15630$ Hz, $a = 0.81 \times 10^5$, and $b = 0.03 \times 10^5$. (d) The data (dots) show the generalized Rabi frequency versus detuning. The solid line represents the fit function (2) with parameters $\Omega_{\text{Rabi}} = 2\pi \cdot 15550$ Hz and $f_{34} = 149\,736\,719.0$ Hz.

where \hbar is the reduced Planck constant and μ is the magnetic dipole moment of the transition (see Supplemental Material [29] for details). The value measured this way is about $\frac{1}{2}$ of one calculated most likely due to the fact that not all details of the metallic construction have been considered.

The fidelity of the population transfer from the $|F = 4, m_F = -4\rangle$ to $|F = 4, m_F = -3\rangle$ levels strongly depends on the coherence properties of the atomic ensemble and achievable Rabi frequency. Thus, both the dephasing time T_2^* and the coherence time T_2 for the transition with frequency f_{43} were examined. This was done using well-established Ramsey [23] and Hahn echo [32] techniques. Figure 3(b) demonstrates the MW pulse sequences used for these experiments. Here, the temperature of the cloud was set to $T \simeq 3.6 \pm 0.2$ μK .

In the Ramsey experiment, atoms were exposed to two resonant MW pulses [“Ramsey” in Fig. 3(b)]. The first was a $\pi/2$ pulse to create a superposition of ground and excited levels, and the second was a $\pi/2$ or $3\pi/2$ pulse to transfer atoms to excited or ground levels, respectively. The results of the two sequences were subtracted to measure the pure coherence-related decay signal. After the pulses, atoms were released, and their number was measured at 500 μs of

expansion. The time between the two pulses τ was varied to observe dephasing of the atomic ensemble. The result is shown in Fig. 4(a); the difference is fitted perfectly with exponential decay $e^{-\tau/T_2^*}$ with dephasing time $T_2^* = 150 \pm 10$ μs .

The echo-type experiment has an additional π pulse in the middle between the two pulses mentioned above [“Echo” in Fig. 3(b)], thus allowing us to remove some dephasing of the atomic ensemble. The idea of such an experiment remains the same unless the roles of the second $\pi/2$ and $3\pi/2$ pulses are switched. The result is shown in Fig. 4(b), and the difference is fitted with $e^{-(\tau/T_2)^\alpha}$ [33], providing an echo-related time of coherence of $T_2 = 500 \pm 20$ μs , with $\alpha = 1.9 \pm 0.2$.

The population decay from the $|F = 3, m_F = -3\rangle$ level was measured at a magnetic field of 5.3 G, as indicated in Fig. 4(c). This measurement was done by applying a π pulse for the transition with frequency f_{43} followed by the same π pulse after some delay time τ , which was varied. After the second π pulse, the trap was released. The measurement of the number of atoms was performed after 2 ms of free expansion of the atomic ensemble by absorption imaging. It is interesting that the population decay is not a single exponential but is rather well described by binary collision decay [34,35]. As a rule, the linear loss γ of a dipole trap is $\sim 1\text{s}^{-1}$, which allows us to fit the decay curve with only binary

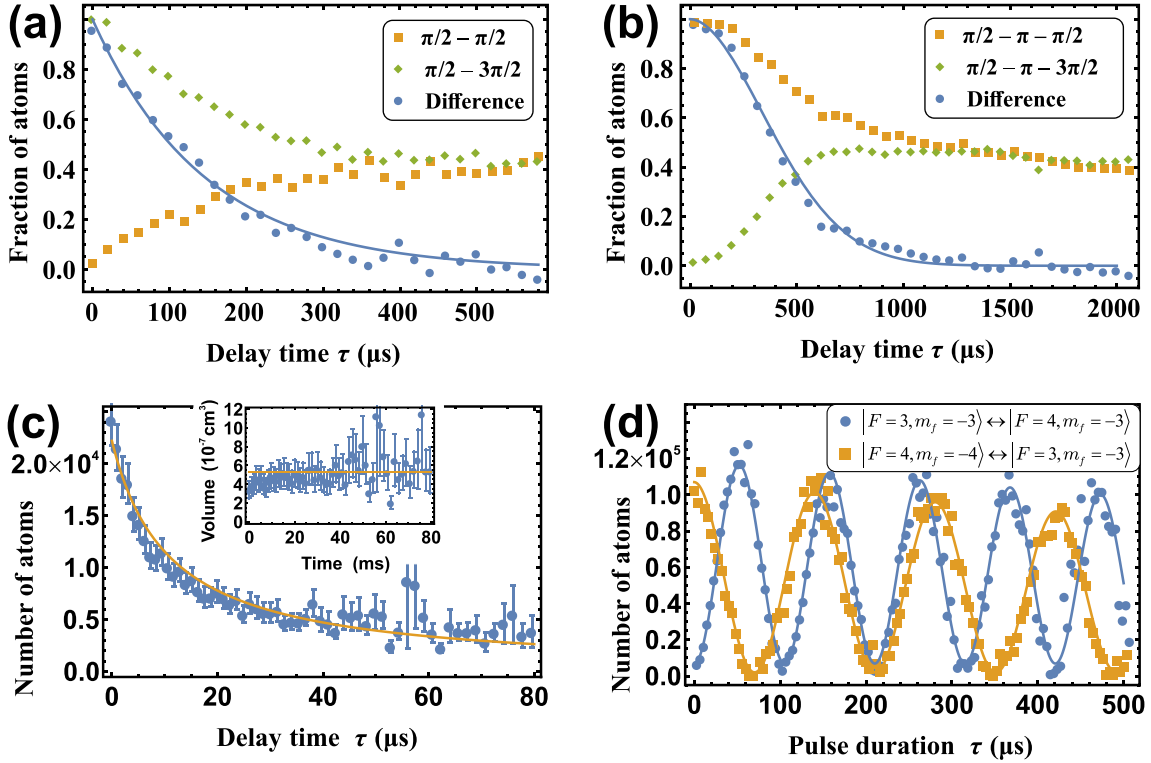


FIG. 4. (a) Data (dots) and fit of the Ramsey sequence. The fit parameter is $T_2^* = 146 \mu\text{s}$. (b) Data (dots) and fit of the Hahn echo sequence. The fit parameters are $T_2 = 502 \mu\text{s}$ and $\alpha = 1.88$. (c) Data (dots) and fit (solid line) of $|F=3, m_F=-3\rangle$ level decay under a magnetic field of 5.3 G with only binary loss, $\beta = 2.23 \times 10^{-9} \text{ cm}^3/\text{s}$. The inset indicates the volume of the atomic cloud versus storage time. (d) Rabi oscillations in the atomic ensemble for the transition with frequency f_{43} (yellow squares) and f_{44} (blue circles). The solid line represents the fit by (5) with parameters $a = 0.52 \times 10^5$, $T_1 = 2513$, $\Omega = 2\pi \cdot 7120 \text{ Hz}$, and $b = 0.02 \times 10^5$ for f_{43} and $a = 0.56 \times 10^5$, $T_1 = 2673$, $\Omega = 2\pi \cdot 9513 \text{ Hz}$, and $b = 0.07 \times 10^5$ for f_{44} .

collisions:

$$N(t) = \frac{N_0}{1 + N_0 \beta^* t}, \quad (4)$$

where N_0 is the initial number of atoms in the trap, and $\beta^* = \beta/V$, where β is a binary collision coefficient and V is the volume of the atomic cloud (see Supplemental Material [29]). The fit parameter was found to be $\beta = 2.23^{+0.8}_{-0.5} \times 10^{-9} \text{ cm}^3/\text{s}$. The contribution of the binary collisions was faster than the linear decay rate, suggesting the presence of dipolar relaxation [36,37], a light-assisted process [34,38–40], or Feshbach resonance [4]. The population decay has a characteristic time of approximately 20 ms, which is much longer than the coherence time, indicating the presence of strong decoherence.

The relatively short coherence time of the hyperfine structure transitions limits how slow the MW pulses could be. Since the transition with frequency f_{33} is much weaker than that with frequency f_{43} [see Fig. 1(a)], it is important to optimize the distribution of the MW field between the two transitions. Thus, to realize population transfer from the $|F=4, m_F=-4\rangle$ level to the $|F=4, m_F=-3\rangle$ level, the dc magnetic field (and, correspondingly, atomic polarization [14]) was tilted (Fig. 1(c) population transfer; the magnetic field is directed along the vector $[-0.76(3), -0.28(1), -0.59(2)]$ with a magnitude of $1.06 \pm 0.04 \text{ G}$ detuned enough from the closest Feshbach resonances for open channel $|F=4, m_F=-4\rangle \rightarrow |F=4, m_F=-4\rangle$ sit-

uated at 1.21 and 1.34 G [12]), such that the Rabi frequencies for the weaker transition with the f_{33} frequency [see Fig. 1(a)] and stronger transition with the f_{43} frequency were approximately the same: $2\pi \cdot (7120 \pm 20) \text{ Hz}$ and $2\pi \cdot (9510 \pm 30) \text{ Hz}$, respectively. The data were fitted with models,

$$\begin{aligned} n &= ae^{-\tau/T_1} [1 \pm \cos(\Omega\tau)] + b, \\ n_{44} &= ae^{-\tau/T_1} [1 + \cos(\Omega\tau)] + b, \end{aligned} \quad (5)$$

where $+$ is selected for level $|F=4, m_F=-4\rangle$ and for level $|F=4, m_F=-3\rangle$. Here, n stands for the population of the corresponding level forming transitions with frequencies f_{33} and f_{43} , a and Ω represent the amplitude and frequency of the Rabi oscillations, parameter T_1 is the population decay time of the atoms in the trap, and b represents the possible background. With these settings, Rabi oscillations for both transitions with f_{33} and f_{43} frequencies were observed by detecting the population of levels with $F=4$ (see Fig. 4(d) and Supplemental Material [29]). With these nearly equal Rabi frequencies, population transfer was realized with the sequence of two π pulses at f_{43} and f_{33} with durations of 67 and 55 μs , respectively, and a 73- μs delay in between. In addition, the trap was turned off during the second pulse as well as 70 μs before and 5 μs after it to reduce trap-related dephasing.

The fidelity of the population transfer from level $|F=4, m_F=-4\rangle$ to level $|F=4, m_F=-3\rangle$ could be

estimated from the contrast of the Rabi oscillations. If some of the population after the first transfer pulse remained in the $|F = 4, m_F = -4\rangle$ level, then the Rabi oscillation would not reach the 0 level at the minimum of the oscillations. It is clear from Fig. 4(d) that practically all the test population transferred after the first π pulse. Nevertheless, if one adds an offset into formula (5), from fitting, one could conclude that $b/(2a + b) = 2\%$. The fit with $b = 0$ is also consistent; therefore, we conclude that no more than 2% remained at level $|F = 4, m_F = -4\rangle$. Similarly, for the Rabi oscillation at frequency f_{33} , if any population remained at level $|F = 4, m_F = -4\rangle$ or another hyperfine level, then the Rabi oscillation would not have full contrast. If any population remained at level $|F = 4, m_F = -4\rangle$, it would again affect the 0 level of the oscillations. The fit gives this level as no more than 6%.

However, since the population at level $|F = 4, m_F = -3\rangle$ is originally nearly 0, the population of $|F = 3, m_F = -3\rangle$ will only appear in the maximum of the oscillations. Thus, to determine by how much the maximum of the oscillations is different from the original number of atoms, the same transfer sequence was repeated twice: with the MW field turned on and off. The change in the number of atoms detected in the ground state with and without MW was no more than 1%. This number gives the amount of how much the amplitude of the oscillations differs from the one originally present and therefore defines the number of atoms in the $|F = 4, m_F = -3\rangle$ level. Thus, at least 93% of the population should be in the $|F = 4, m_F = -3\rangle$ level. This does not include any factors related to the purity of the original level; therefore, the actual fidelity of the transfer should be higher. Therefore, the transfer fidelity is over 93%.

High-fidelity microwave manipulations of the thulium ground-state open the range of possibilities on implementation of quantum simulations with thulium atoms, enabling easily controlled multistate gas mixtures with selectively controlled interactions. This could be potentially realized via Feshbach resonances, which are expected to be different for different magnetic states as well as for cross-state collisions due to distinct entrance channels [41]. Other opportunities, similar to spin-dependent optical lattices [42–44], arise from strong dependence of optical lattice depth on magnetic states due to the complex behavior of atom polarizability [27].

IV. CONCLUSION

Population transfer from the $|F = 4, m_F = -4\rangle$ level of a thulium-169 cold atomic ensemble to $|F = 4, m_F = -3\rangle$ was demonstrated by the consequent application of two π pulses between hyperfine levels of the ground state with fidelity $F > 93\%$. The transfer was performed using a specially designed MW antenna. The dephasing and coherence times of the intermediate-state higher hyperfine components of the thulium atom were measured to be 150 and 500 μs , respectively.

ACKNOWLEDGMENTS

The MW antenna design, fabrication, and experimental investigation were supported by Russian Science Foundation Grant No. 19-19-00693. The manipulation of the ultracold thulium atom ground state and all optical experiments were supported by Russian Science Foundation Grant No. 18-12-00266.

-
- [1] I. M. Georgescu, S. Ashhab, and F. Nori, *Rev. Mod. Phys.* **86**, 153 (2014).
 - [2] T. Lahaye, C. Menotti, L. Santos, M. Lewenstein, and T. Pfau, *Rep. Prog. Phys.* **72**, 126401 (2009).
 - [3] P. M. Duarte, R. A. Hart, T. L. Yang, X. Liu, T. Paiva, E. Khatami, R. T. Scalettar, N. Trivedi, and R. G. Hulet, *Phys. Rev. Lett.* **114**, 070403 (2015).
 - [4] C. Chin, R. Grimm, P. Julienne, and E. Tiesinga, *Rev. Mod. Phys.* **82**, 1225 (2010).
 - [5] E. T. Davletov, V. V. Tsyganok, V. A. Khlebnikov, D. A. Pershin, D. V. Shaykin, and A. V. Akimov, *Phys. Rev. A* **102**, 011302(R)(2020).
 - [6] M. Lu, N. Q. Burdick, S. H. Youn, and B. L. Lev, *Phys. Rev. Lett.* **107**, 190401 (2011).
 - [7] K. Aikawa, A. Frisch, M. Mark, S. Baier, A. Rietzler, R. Grimm, and F. Ferlaino, *Phys. Rev. Lett.* **108**, 210401 (2012).
 - [8] T. Maier, H. Kadau, M. Schmitt, M. Wenzel, I. Ferrier-Barbut, T. Pfau, A. Frisch, S. Baier, K. Aikawa, L. Chomaz, M. J. Mark, F. Ferlaino, C. Makrides, E. Tiesinga, A. Petrov, and S. Kotochigova, *Phys. Rev. X* **5**, 041029 (2015).
 - [9] T. Maier, I. Ferrier-Barbut, H. Kadau, M. Schmitt, M. Wenzel, C. Wink, T. Pfau, K. Jachymski, and P. S. Julienne, *Phys. Rev. A* **92**, 060702(R) (2015).
 - [10] K. Baumann, N. Q. Burdick, M. Lu, and B. L. Lev, *Phys. Rev. A* **89**, 020701(R) (2014).
 - [11] E. Lucioni, L. Tanzi, A. Fregosi, J. Catani, S. Gozzini, M. Inguscio, A. Fioretti, C. Gabbanini, and G. Modugno, *Phys. Rev. A* **97**, 060701 (2018).
 - [12] V. A. Khlebnikov, D. A. Pershin, V. V. Tsyganok, E. T. Davletov, I. S. Cojocar, E. S. Fedorova, A. A. Buchachenko, and A. V. Akimov, *Phys. Rev. Lett.* **123**, 213402 (2019).
 - [13] T. H. Loftus, T. Ido, M. M. Boyd, A. D. Ludlow, and J. Ye, *Phys. Rev. A* **70**, 063413 (2004).
 - [14] V. V. Tsyganok, V. A. Khlebnikov, E. S. Kalganova, D. A. Pershin, E. T. Davletov, I. S. Cojocar, I. A. Luchnikov, A. V. Berezhutskii, V. S. Bushmakina, V. N. Sorokin, and A. V. Akimov, *J. Phys. B: At., Mol. Opt. Phys.* **51**, 165001 (2018).
 - [15] V. Tsyganok, D. Pershin, V. Khlebnikov, E. Davletov, and A. Akimov, *J. Exp. Theor. Phys.* **128**, 199 (2019).
 - [16] I. I. Rabi, *Phys. Rev.* **51**, 652 (1937).
 - [17] M. S. Silver, R. I. Joseph, C. N. Chen, V. J. Sank, and D. I. Hault, *Nature* **310**, 681 (1984).
 - [18] B. T. Torosov and N. V. Vitanov, *Phys. Rev. A* **97**, 043408 (2018).
 - [19] M. H. Leviti and R. Freeman, *J. Magn. Reson.* **33**, 473 (1979).
 - [20] M. Garwood and L. Delabarre, *J. Magn. Reson.* **153**, 155 (2001).

- [21] N. V. Vitanov, A. A. Rangelov, B. W. Shore, and K. Bergmann, *Rev. Mod. Phys.* **89**, 015006 (2017).
- [22] S. A. Snigirev, A. A. Golovizin, G. A. Vishnyakova, A. V. Akimov, V. N. Sorokin, and N. N. Kolachevskii, *Quantum Electron.* **42**, 714 (2012).
- [23] J. E. Thomas, P. R. Hemmer, S. Ezekiel, C. C. Leiby, R. H. Picard, and C. R. Willis, *Phys. Rev. Lett.* **48**, 867 (1982).
- [24] D. Gignlberger and S. Penselin, *Z. Phys.* **199**, 244 (1967).
- [25] W. J. Childs, H. Crosswhite, L. S. Goodman, and V. Pfeufer, *J. Opt. Soc. Am. B* **1**, 22 (1984).
- [26] D. A. Pershin, V. V. Tsyganok, V. V. Yaroshenko, V. A. Khlebnikov, E. T. Davletov, E. L. Svechnikov, V. N. Sorokin, P. V. Kapitanova, and A. V. Akimov, *Bull. Lebedev Phys. Inst.* **45**, 377 (2018).
- [27] V. V. Tsyganok, D. A. Pershin, E. T. Davletov, V. A. Khlebnikov, and A. V. Akimov, *Phys. Rev. A* **100**, 042502 (2019).
- [28] W. Ketterle, M. R. Andrews, K. B. Davis, D. S. Durfee, D. M. Kurn, M.-O. Mewes, and J. van Druten, *Phys. Scr.* **T66**, 31 (1996).
- [29] See Supplemental Material at <http://link.aps.org/supplemental/10.1103/PhysRevA.102.043114> for details of absorption imaging, g factors, calibration MW field, and decay fit.
- [30] D. M. Sazonov, *Microwave Circuits and Antennas* (Mir Publishers, Moscow, 1990).
- [31] V. S. Letokhov and V. P. Chebotayev, *Nonlinear Laser Spectroscopy*, 1st ed. (Springer-Verlag, Berlin, 1977).
- [32] E. L. Hahn, *Phys. Rev.* **80**, 580 (1950).
- [33] P. L. Stanwix, L. M. Pham, J. R. Maze, D. Le Sage, T. K. Yeung, P. Cappellaro, P. R. Hemmer, A. Yacoby, M. D. Lukin, and R. L. Walsworth, *Phys. Rev. B* **82**, 201201(R) (2010).
- [34] I. S. Cojocaru, S. V. Pyatchenkov, S. A. Snigirev, I. A. Luchnikov, E. S. Kalganova, G. A. Vishnyakova, D. N. Kublikova, V. S. Bushmakina, E. T. Davletov, V. V. Tsyganok, O. V. Belyaeva, A. Khoroshilov, V. N. Sorokin, D. D. Sukachev, and A. V. Akimov, *Phys. Rev. A* **95**, 012706 (2017).
- [35] R. Grimm, M. Weidemüller, and Y. B. Ovchinnikov, *Adv. At., Mol. Opt. Phys.* **42**, 95 (2000).
- [36] S. Hensler, J. Werner, A. Griesmaier, P. O. Schmidt, A. Görlitz, T. Pfau, S. Giovanazzi, and K. Rzażewski, *Appl. Phys. B* **77**, 765 (2003).
- [37] F. H. Mies, C. J. Williams, P. S. Julienne, and M. Krauss, *J. Res. Natl. Inst. Stand. Technol.* **101**, 521 (1996).
- [38] A. Fuhrmanek, R. Bourgain, Y. R. P. Sortais, and A. Browaeys, *Phys. Rev. A* **85**, 062708 (2012).
- [39] G. Telles, L. Marcassa, S. Muniz, S. Miranda, A. Antunes, C. Westbrook, and V. Bagnato, *Phys. Rev. A* **59**, R23 (1999).
- [40] M. S. Hamilton, A. R. Gorges, and J. L. Roberts, *J. Phys. B: At., Mol. Opt. Phys.* **45**, 095302 (2012).
- [41] S. Kotochigova, *Rep. Prog. Phys.* **77**, 093901 (2014).
- [42] A. J. Daley, M. M. Boyd, J. Ye, and P. Zoller, *Phys. Rev. Lett.* **101**, 170504 (2008).
- [43] P. J. Lee, M. Anderlini, B. L. Brown, J. Sebby-Strabley, W. D. Phillips, and J. V. Porto, *Phys. Rev. Lett.* **99**, 020402 (2007).
- [44] O. Mandel, M. Greiner, A. Widera, T. Rom, T. W. Hänsch, and I. Bloch, *Phys. Rev. Lett.* **91**, 010407 (2003).